Vertical high emission in photonic crystal nanocavities by band-folding design

Nguyen-Vi-Quynh Tran*
Thales Research and Technology, Route Départementale 128, 91767 Palaiseau, France
and Nanyang Technological University, 50 Nanyang Avenue, 639798 Singapore, Singapore

Sylvain Combrié,† Pierre Colman, and Alfredo De Rossi
Thales Research and Technology, Route Départementale 128, 91767 Palaiseau, France

Ting Mei
Nanyang Technological University, 50 Nanyang Avenue, 639798 Singapore, Singapore
(Received 8 February 2010; published 12 August 2010)

We demonstrate reshaping of the radiation pattern emitted from photonic crystal nanocavities. More than 80% of the radiated power can be collected by an optics having numerical aperture of 0.6. This technique is very robust against disorders. The band folding method can be applied to almost any kind of cavity in order to reach stronger and more directive emission.

DOI: 10.1103/PhysRevB.82.075120 PACS number(s): 42.70.Qs, 42.60.Da, 42.55.Tv, 41.20.Jb

I. INTRODUCTION

Photonic crystal (PhC) cavities have been proven to confine the optical field in a very small volume (V) efficiently, with reported quality factors (Q) on the order of 1 million.[1–7] Large Q/V ratio enhances significantly the Purcell factor[8] making PhC cavities suitable candidates for cavity quantum electrodynamics (cavity QED), single photon sources, and nanolasers.[9–12] The efficient vertical extraction from the cavity is also a highly desired property but difficult to achieve because the radiation pattern of most PhC cavities is very broad. Vertical extraction is also crucial for future photonic integrated circuits (coupling to fiber, multilayer structures)[13] and enables large scale fabrication of optical emitters (e.g., vertical-cavity surface-emitting laser).

Some designs have been proposed by several groups[14,15] in order to improve the radiation pattern and the collection efficiency but very few experimental results have been reported so far.[16,17] In addition, these designs are specific to a particular kind of cavity. We have introduced the photonic band folding design concept and demonstrated vertical emission with a bell-shaped radiation pattern. We have achieved experimentally[18] more than 40% collection efficiency using optics with numerical aperture NA=0.6.

In this paper, we demonstrate the generality of the band-folding concept and apply it to many types of cavities. We will first recall the photonic band-folding principle and apply it to one-dimensional (1D) PhC structure. Then we will demonstrate the control of the emission pattern on two-dimensional (2D) PhC structure such as $L3$, heterostructure, H0, and hexapole. To conclude we will investigate the robustness of the technique against disorder.

II. BAND-FOLDING PRINCIPLE

For the sake of simplicity, let us consider the 1D cavity composed of two Bragg mirrors, as shown in Fig. 1(b). Once optimized for high Q factor, minimizing the out-coupling radiation, the field distribution in the reciprocal space, Fig. 1(a), has a peak at the first Brillouin zone (BZ) but it vanishes at the center ($k_x=0$, corresponding to the perpendicular direction). Most of the radiation arises from the tails of this peak, located inside the light cone and close to the light line. That explains why the far field is usually broad and most of the radiation is emitted at grazing angles [see sketch in Fig. 1(c) showing typical emission of 2D PhC cavity].

Let us introduce a subharmonic in the lattice with period $\Pi=2a$ [Fig. 1(e)]. Consequently, the main peak in the reciprocal space is folded with respect to $k_x=\frac{\pi}{2a}$ and a replica appears at $k_x=0$, Fig. 1(d). The far field is modified in such way that the major emission is now along the vertical direction [Fig. 1(f)].

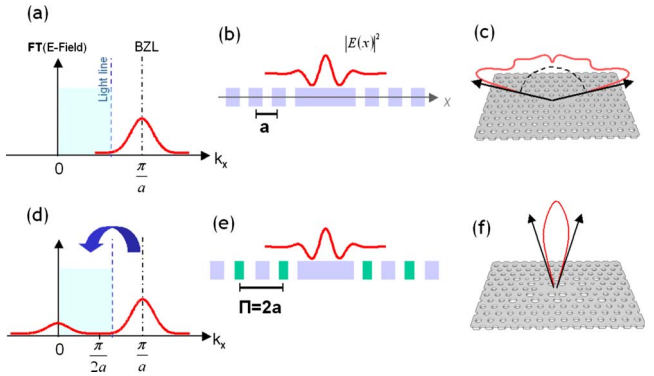

FIG. 1. (Color online) Principle of band folding: schematic of a 1D cavity (b). Corresponding E-field distribution in the k space (a) with minima at $k_x=0$ after Q-factor optimization. Modified design with additional subharmonic modulation (e). Resulting replica appearing at $k_x=0$ consequently to band-folding (d). Sketch of typical emission of 2D PhC cavities when optimized to achieve high Q factor (c) and with addition to the subharmonic modulation (f) improving the directivity of the vertical emission.

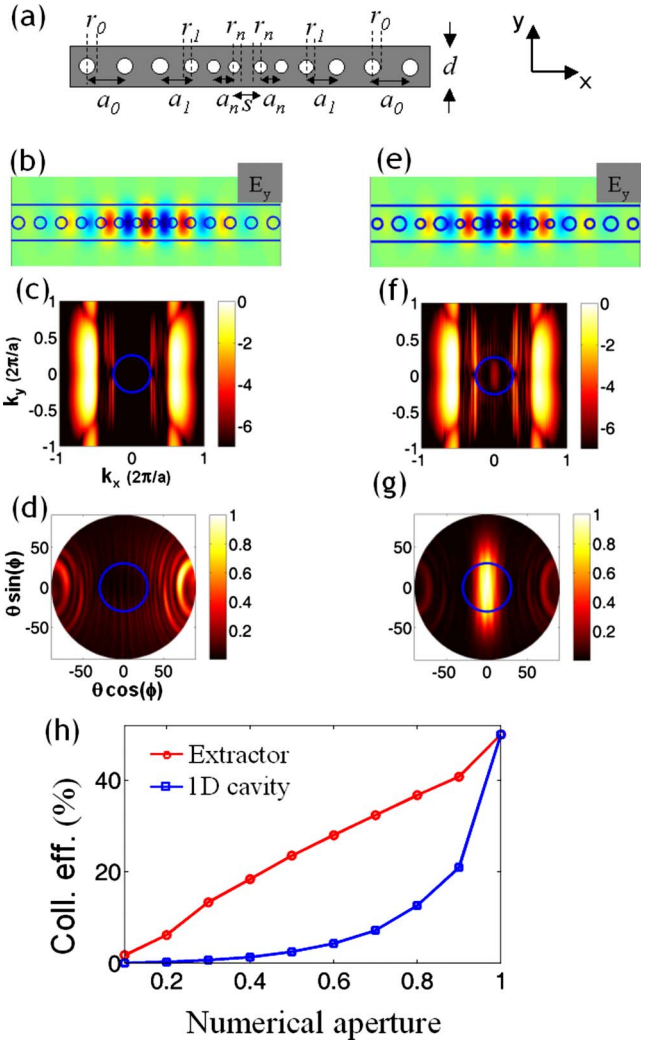

FIG. 2. (Color online) 1D PhC cavity: schematic of the 1D PhC cavity design used for band folding implementation (a). Calculated *E*-field distribution represented in real space (b) and *k* space (c). Associated emission diagram with no significant radiated vertical component (d). *E*-field distribution of the modified design with subharmonic modulation in real (e) and reciprocal (f) spaces. Corresponding radiation pattern with directive vertical emission (g). Comparison of collection efficiency as a function of the NA for regular 1D cavity (squares) and new "extractor" design (open circles) (h). The blue circle in (d) and (g) represents the collection angle of optics having numerical aperture NA=0.5.

III. 1D PhC CAVITY

To illustrate the concept with a realistic example, we consider the 1D PhC structure shown in Fig. 2(a) and described in Refs. 19 and 20. It consists of a dielectric nanowire ($\varepsilon=11.4$) suspended in air and perforated by holes. The 1D PhC is composed of 40 holes with period a_0 and normalized radius $r_0=0.27a_0$. The cavity is formed by a linear gradient of the radius of the $2n$ inner holes. In our simulations, $n=7$ and $r_m=r_0-0.01m$ with $m=1,2,\ldots,n$. The distance a_m between two adjacent holes also varies following the rule: $a_m=r_m/0.27$. The parameter s, distance between the two inner holes, was set to $s=a_n$ but can be detuned for a further optimization of the Q factor. Maxwell equations are solved in three dimensions (3D) using our own parallel implementation of the finite differences in time domain (FDTD) method[21] including perfectly matched layers[22] as boundary conditions. Moreover, subpixel smoothing of the dielectric function[23] is used to improve accuracy. The thickness and the width of the nanowire were set, respectively, to $h=0.65a_0$ and $d=1.5a_0$. The electric field (E_y) of the resonant mode, as shown in Fig. 2(b), is well confined leading to a theoretical Q factor of about 3×10^5. Its component, parallel to the slab surface, is now represented [Fig. 2(c)] in the reciprocal space (i.e., the spatial Fourier transform). The quasiabsence of field inside the light cone (represented by a circle) compared to the rest of the field confirms this good confinement. The emission diagram of the cavity can be calculated using an approximation suitable for planar structures.[14,18,24,25] It relates the electric and magnetic fields parallel to the surface to the radiation pattern $\sigma(\theta,\phi)$ through

$$\sigma \approx A \int\int_{|\vec{k}_\parallel|<\omega/c} |\tilde{H}_y + \tilde{E}_x/\eta_0|^2 + |\tilde{H}_x - \tilde{E}_y/\eta_0|^2 dk_\parallel^2. \quad (1)$$

Here $A=\omega^2/(8\pi\eta_0 c^2)$ and $\sigma(\theta,\phi)$ is defined as the normalized radiated power, i.e., $\sigma(\theta,\phi)=P(\theta,\phi)/(W\omega_0)$ with $P(\theta,\phi)$ the power, W the energy in the mode, and η_0 the vacuum impedance. Importantly, as the relevant mode in dielectric 2D PhCs is quasi-TE (transverse electric), the dominant contribution is from the electric field.[24] As shown in Fig. 2(d), the emission occurs at grazing angles with almost no contribution at the vertical direction.

In order to modify the radiation pattern, we introduce a subharmonic modulation with period $\Pi=2a$. This was implemented by changing periodically the hole radius, alternating successively an increase of $+\Delta r$ and a reduction of $-\Delta r$, starting with the small radius at the edge of the cavity. We chose a large modulation factor of $\Delta r=0.04a$ to stress the band-folding effect and see it more clearly. The effect on the mode profile is not appreciable in the real space [Fig. 2(e)] whereas in the reciprocal space the onset of a local maximum at Γ [Fig. 2(f)], replica of the main peak at K ($k_x=\frac{\pi}{a}$), is apparent. That change corresponds to a drastic reshaping of the far-field pattern, shown in Fig. 2(g). The far field is now directed vertically with a reduced angular spread ($\sim30°$) on the *XZ* plane. As a note, the angular spread on the *YZ* plane is broader and only depended on the wire width and cannot be controlled through PhC design.

The Q factor of the modified structure ($Q_{ex}=3000$) is lower compared to the original structure ($Q_0=3\times10^5$) as the optical extraction is increased. In contrast to nonoptimized cavities, here the fraction of radiation which is funneled into the mode centered in $k=0$ is large and approximately ($1-\frac{Q_{ex}}{Q_0}\simeq99\%$). Thus, the larger the Q factor of the original cavity, the larger the potential extraction efficiency or the Q factor allowed for the "extractor." The Q factor of the modified structure can be tailored depending of the specific application by adjusting the subharmonic modulation strength.

The normalized collection efficiency, i.e., the amount of radiation which can be collected with an optics with numerical aperture NA is

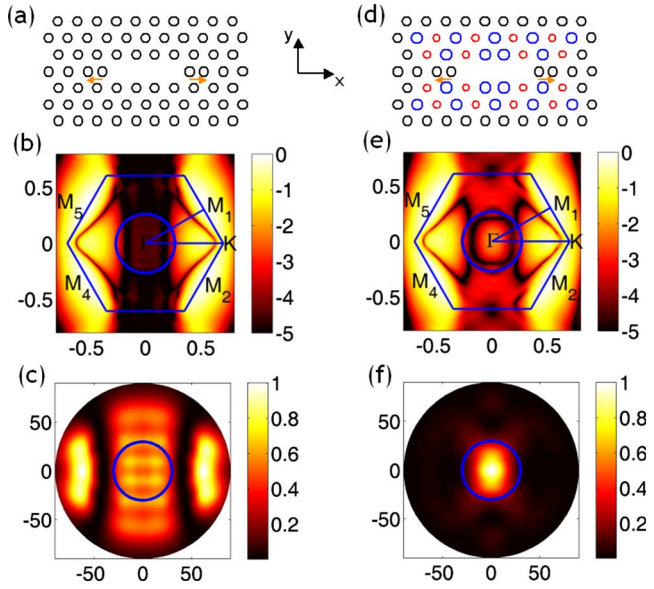

FIG. 3. (Color online) $L3$ cavity: schematic of the $L3$ cavity with standard design (a) and with implementation of the band folding (d) through additional sub-harmonic modulation. Calculated E-field distribution in the k space without (b) and with (e) band folding. Corresponding radiation pattern with broad emission for the standard $L3$ design (c) and highly directive for the modified (f).

$$\sigma(\mathrm{NA}) = \int_{2\pi} \int_{\theta=0}^{\arcsin(\mathrm{NA})} \sigma(\theta,\phi) d\theta d\phi. \qquad (2)$$

This is plotted in Fig. 2(h). Because of the symmetry of the PhC slab, the maximum theoretical collection is 50%. It is apparent that the collection efficiency of the extractor is far better (one order of magnitude improvement with NA $=0.25$) than that of the original cavity.

IV. EXTRACTOR MADE FROM L-TYPE CAVITIES

Let us now consider the well-known $L3$ cavity, broadly used for QED,[26] all-optical processing[27] and filtering.[28] It is composed of three-in-line missing holes [see Fig. 3(a)]. We have used the following parameters: lattice constant a, slab thickness $h=0.639a$, hole radius $r_n=0.29a$, hole shifting $s=0.15a$, $\varepsilon=11.4$. The theoretical Q factor is about 50 000 with resonance wavelength at $\lambda=3.76a$.

The distribution of the electric field in reciprocal space of the cavity is shown in Fig. 3(b) and calculated in the same way as in the previous section. The field intensity peaks at the four M points of the first BZ. The corresponding far field is shown in Fig. 3(c) and as expected, the emission is directed along two main lobes at about 70° from the vertical direction. That implies that a small fraction of the emitted light can be collected by usual optics with NA=0.5.

The vertical emission of 2D PhC cavity can be modified by introducing a subharmonic period. Due to the symmetries of the E field in the k space, two gratings are superimposed. They are obtained by modulating the radius of the holes by $\Delta r=0.01a$ around the cavity. The modified structure is shown in Fig. 3(d).

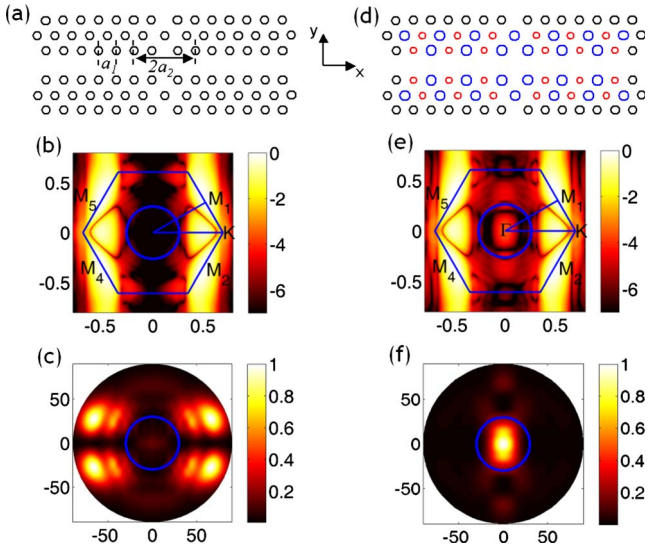

FIG. 4. (Color online) Heterostructure cavity: standard design (a) with two elongated periods forming the heterostructure cavity. Optimized design (d) for vertical emission including the new subharmonic periodicity. E-field distribution in reciprocal space for the original design (b) and the modified one (e). Associated emission diagrams, respectively (c) and (f).

Figure 3(e), shows a peak at Γ. The far field is reshaped drastically [Fig. 3(f)] and radiation is emitted along the vertical axis, most of it within a collection angle of NA=0.5 (blue circle). The increased emission entails the drop of the Q factor from 50 000 to 13 000. The fraction of radiation going into the bell-shaped mode centered in $k=0$ is approximately $(1-\frac{Q_{ex}}{Q_0} \simeq 74\%)$. Figures 3(c) and 3(f) show the radiation of the original cavity and of the new structure, respectively. In contrast with the 1D structure, the far field is almost circular as the divergence on the YZ plane is reduced as well. That possibility is enabled in 2D PhC. Most of energy is directed within an angle of 30°, represented by the circle. We performed the calculation only on one-half space and found that about 30% of the total emission energy can be captured with an optics having numerical aperture of NA=0.5. This captured amount can be doubled (i.e., 60%) by using an appropriate mirror under the cavity as suggested in Ref. 14 in order to reflect all emission toward the top of the cavity.

The case of $L5$ cavity can be analyzed in a similar way. We have indeed demonstrated theoretically and experimentally a strong improvement of directivity from the $L5$ cavity.[18]

Let us consider the so-called heterostructure cavity.[2] It is composed by a section of waveguide of period a_1 with a local elongation along the missing row of two larger periods a_2. The longitudinal confinement results from the cutoff of the waveguide with the smallest period [Fig. 4(a)]. This kind of cavity allows very large Q factor $(Q_{int}=2.5\times10^6)$. The distribution of the E field in the k space [Fig. 4(b)] is similar to the $L3$ cavity, however, the far field is broader [Fig. 4(c)], with four lobes at very large angle and with less power in the vertical emission compared to the $L3$. That reason limited the

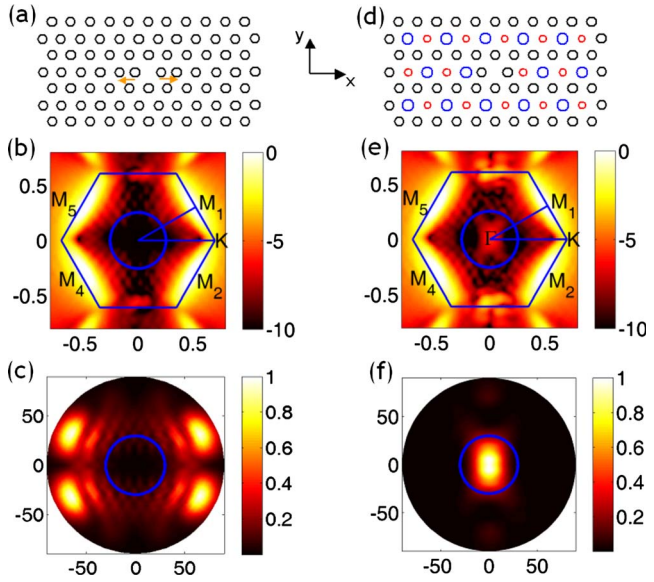

FIG. 5. (Color online) H0 cavity: schematic of the zero-point defect (H0) cavity without (a) and with (d) the band-folding structure. Associated E field in reciprocal space (b) and (e), and emission diagrams (c) and (f).

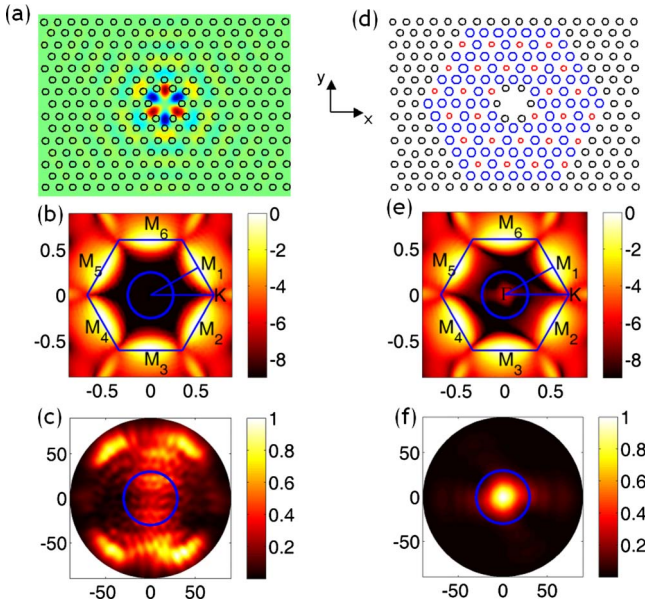

FIG. 6. (Color online) Hexapole cavity: calculated Hz-field distribution of the hexapole cavity (a). Corresponding E-field distribution in k space (b) and far-field pattern (c). Schematic of the new design (d) including the band-folding principle. Associated field distribution in reciprocal space (e) and radiation diagram (f) showing directive emission perpendicular to the membrane.

interest of this design for light-matter interaction investigations,[11] despite the potential large Q factor.

A new subharmonic period is added in the structure as shown in Fig. 4(d). A modulation of the hole radius of $\Delta r=0.01a$ is introduced in the cavity, decreasing the Q factor to $Q=48\,000$. A replica appears at $k=0$ in the reciprocal space [Fig. 4(e)], leading to a Gaussian vertical emission [Fig. 4(f)].

The design investigated so far considers cavity modes with an even symmetry of the Ey field with respect to the YZ plane. In order to control the radiation of odd modes with respect to the same symmetry plane, the subharmonic has to be shifted by a half grating period along X (π shift). Let us consider the case of the H0 cavity,[29] resulting from a local modification of the crystal to create a donor mode in the band gap. Two holes are moved by $s=0.16a$ in opposite direction along ΓK [see Fig. 5(a)]. Using the following parameters, $h=0.72a$ and $r=0.30a$, a frequency resonance at $\lambda=3.92a$ and a Q factor of $Q=548\,000$ have been found by 3D FDTD calculation. The emission is very broad and mainly composed of four lobes at very large angles.

Now, we introduce the subharmonic period [blue/red holes, see Fig. 5(d)] and we note that it has an odd symmetry with respect to YZ plane. The radius of the holes is modified by $\Delta r=0.02a$. The radiation is directed vertically and forms a bell-shaped beam. The increase in extraction, controlled by Δr, resulted into a decrease in the Q factor to 19 000.

V. VERTICAL EMISSION FROM CAVITY WITH AN HEXAPOLE MODE

Single-defect-type cavities have been studied by different groups.[4,14,17] In particular, the hexapole mode has a sixfold symmetric field. After optimization of the cavity design, this mode can exhibit very high theoretical Q factor[30] up to 3×10^6. This optimization can be done by different ways, for instance by decreasing the radius or by shifting the inner holes or both of them. Recently, highly directive emission has been shown[14,17] with this cavity mode by breaking the symmetry. This was obtained by enlarging two over the six inner holes. However, this design appears very sensitive to structural disorder introduced during fabrication because the directivity of the field is critically controlled by the exact position and diameters of two holes. When applying, the band-folding technique, the modification is spread over a larger number of holes, thereby decreasing the sensitivity to disorder. The initial design parameters are similar to that reported in Ref. 4 with the six inner holes moved outward. The H_z-field distribution of hexapole mode is shown in Fig. 6(a). The calculated corresponding Q factor is 660 000.

The sixfold symmetry of the mode [Fig. 6(a)] corresponds to six peaks in the reciprocal space [Fig. 6(b)] at M_1, M_2, M_3, M_4, M_5, and M_6. Subharmonic grating vectors are applied along the axis M_1M_4, M_2M_5, and M_3M_6 [Fig. 6(d)].

The corresponding far fields are calculated using formula (1) and shown in Figs. 6(c) and 6(f). The very broad emission pattern of the original structure [Fig. 6(c)] is reshaped into a sharp and extremely well-confined beam. In contrast to the other designs, in particular, the 1D cavity producing an elliptical vertical beam, this design allows an almost perfectly circular beam, owing to the original sixfold symmetry of the mode. The Q factor is reduced to 48 000 when $\Delta r=0.02a$. The calculated far field in Fig. 6(c) lacks of the sixfold symmetry of the structure. That is a numerical artifact introduced by the use of the rectangular FDTD grid. As the far field depends on the residual near field within the light

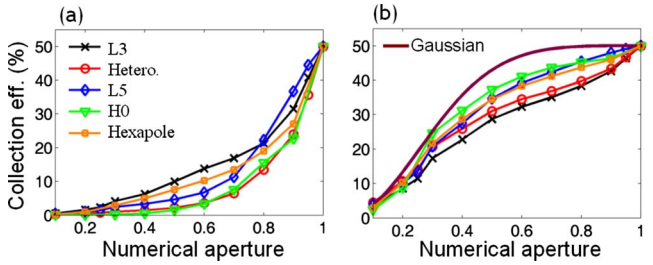

FIG. 7. (Color online) Collection efficiency as a function of NA: standard designs require large NA (left) whereas the modified designs improve collection efficiency for the same NA (right).

cone, that effect is exacerbated in the case of the optimized hexapole cavity (prior to band folding).

VI. COMPARISON OF THE COLLECTION EFFICIENCIES

Let us now have a direct comparison of all the designs considered here above. We will take the collection efficiency σ(NA) as the relevant benchmark, which is calculated as a function of the numerical aperture through formula (2). Let us consider the original cavity designs [Fig. 7(a)]. In any case, the collection efficiency follows a similar trend: quite small efficiency until NA approaches 1. Now, we compare with the modified structures [Fig. 7(b)]. The collection efficiency increases very fast with NA and is more than acceptable for NA $\sim$ 0.3, which is easy to achieve with simple optical systems. With an optics having numerical aperture of NA=0.6, we can collect an amount of almost 40% of the radiation from the heterostructure, H0, hexapole mode extractors, and more than 30% from the *L*3, *L*5 extractors; whereas the original designs only reach, at the maximum, 15% of collection efficiency.

The near field at the surface of PhC membrane cavities is strongly confined and extends over a few photonic lattice periods (e.g., the size is typically 1.5 μm $\times$ 0.5 μm $(1/e^2)$ for the *L*3 and slightly more or less for the other cavities). A Gaussian beam with waist of similar size would diverge with angle $(1/e^2)$ of about 30°, which is quite close to the divergence of the beam radiated by the PhC cavity. Efficient mode matching with a single mode fiber was reported in our previous work[18] for *L*5 cavity and the picture is still valid for the cavities discussed here, particularly the H0 and the hexapole.

VII. EXTRACTOR WITH ARTIFICIAL-INDUCED DISORDERS

A crucial issue is the resilience of the design against structural disorder resulting from fabrication. That is crucial for practical implementation of these concepts. In order to demonstrate the robustness of our design based on band folding, we have deliberately introduced disorder in our *L*5 and H0 cavities optimized for the vertical emission. The perturbation consists of a random fluctuation δr of the hole radius r_n, following the normalized distribution: $r_n = r_0(1+\delta r S)$, with r_0 the size of the nominal hole radius. S is a random variable with distribution $P(S) = \frac{1}{\sqrt{2\pi}} e^{-S^2/2}$.

We ran four instances of the disordered structure for each value of $\delta r/r_0$ (1%, 2%, 3%, 4%, and 5%). Here, we focus on the *L*5 extractor.

Figure 8(a) shows the collection efficiency as a function of NA and its standard deviation with $\delta r/r_0 = 5\%$; which probably overstates disorder. Thus, we conclude that the beaming properties of that cavity design are almost insensitive to disorder associated to state-of-the-art fabrication, as apparent in far-field patterns shown in Fig. 8(c). Similar results have been obtained with the other designs reported in this paper.

In addition to the impact of the fluctuation of the holes size, we further investigated the robustness of the design against the mispositioning of the holes: $\mathbf{X} = \mathbf{X}_0 + \delta x(\mathbf{x}S_x + \mathbf{y}S_y)$ with $S_{x,y}$ two independent variables defined as S. For each value of δx, we ran four simulation instances. Figure 9(a) compares the collection efficiency from a perfect and disordered extractor cavity with $\delta x = 1\%a$ and $2\%a$ (e.g., 4 nm and 8 nm) with the reference cavity. The typical near and far fields for the disordered

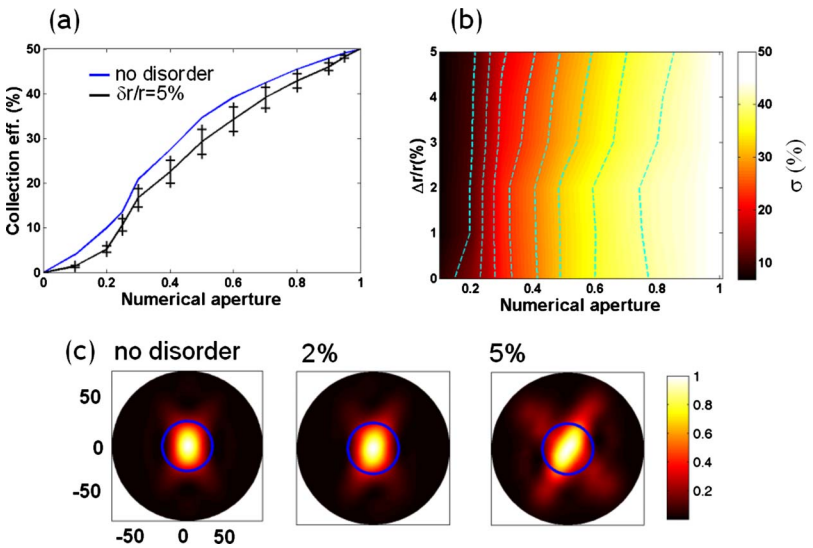

FIG. 8. (Color online) Impact of disorder on radius: plot of the collection efficiency (a) versus the NA for the *L*5 extractor with and without disorder. Pseudocolor map (b) showing the collection efficiency as a function of the amount of disorder and the NA. Typical far-field patterns (c) of a *L*5 extractor for increasing disorder.

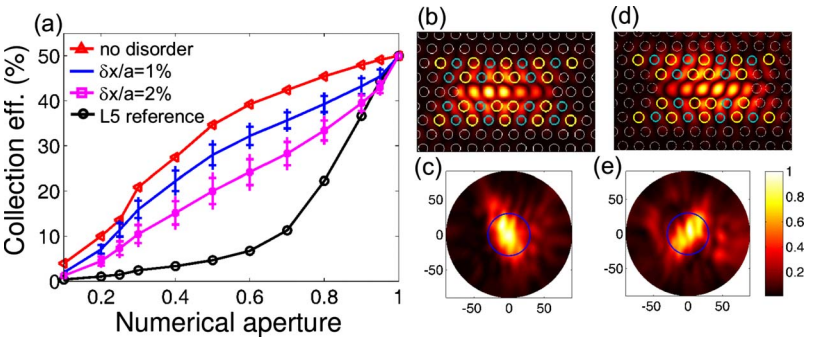

FIG. 9. (Color online) Impact of disorder on position: plot of the collection efficiency (a) versus the NA for the *L5* extractor with and without disorder. Calculated *E*-field distribution of the *L5* extractor and related far-field patterns for 1% (b) and (c), and 2% (d) and (e), respectively.

structures are also reported [Figs. 9(b)–9(e)]. Here, the impact on the near field is apparent, but, still, the beaming properties are not affected drastically [Figs. 9(c) and 9(e)] and therefore the extractions is still far better than that of the reference cavity. We also note that we exaggerated the extent of disorder on purpose.

VIII. DISCUSSION AND CONCLUSION

We have generalized the concept of band folding for improving the directivity of the emission of PhC cavities. That concept, which we demonstrated experimentally in Ref. 18, was implemented on different kinds of PhC cavities, 1D, *L*-type, heterostucture, H0, and hexapole. In all cases we succeeded in improving directivity and collection efficiency dramatically so that simple optics with NA 0.6 can be used to extract most of the radiation. We have also investigated the robustness of the design against fabrication defects and found that even with quite pessimistic guess on disorder, the directivity and collection efficiency are preserved. We believe this is due to the fact that the design is based on a distributed modification of the original structure and it does not depend on some design features (e.g., single holes) critically.

ACKNOWLEDGMENTS

This work was partly funded by the European Commission within the project QPhoton under Contract No. IST029283 and by French National Research Agency (QSWITCH project) and by National Research Foundation, Singapore (Project No. NRF-G-CRP 2007-01).

*tnvquynh@ntu.edu.sg
†sylvain.combrie@thalesgroup.com

[1] S. Noda, A. Chutinan, and M. Imada, Nature (London) **407**, 608 (2000).
[2] B.-S. Song, S. Noda, T. Asano, and Y. Akahane, Nat. Mater. **4**, 207 (2005).
[3] E. Kuramochi, M. Notomi, S. Mitsugi, A. Shinya, T. Tanabe, and T. Watanabe, Appl. Phys. Lett. **88**, 041112 (2006).
[4] T. Tanabe, A. Shinya, E. Kuramochi, S. Kondo, H. Taniyama, and M. Notomi, Appl. Phys. Lett. **91**, 021110 (2007).
[5] K. Nozaki and T. Baba, Appl. Phys. Lett. **88**, 211101 (2006).
[6] E. Weidner, S. Combrié, N.-V.-Q. Tran, A. De Rossi, J. Nagle, and S. Cassette, Appl. Phys. Lett. **89**, 221104 (2006).
[7] S. Combrié, A. De Rossi, N.-V.-Q. Tran, and H. Benisty, Opt. Lett. **33**, 1908 (2008).
[8] E. M. Purcell, H. C. Torrey, and R. V. Pound, Phys. Rev. **69**, 37 (1946).
[9] W.-H. Chang, W.-Y. Chen, H.-S. Chang, T.-P. Hsieh, J.-I. Chyi, and T.-M. Hsu, Phys. Rev. Lett. **96**, 117401 (2006).
[10] A. Badolato, K. Hennessy, M. Atature, J. Dreiser, E. Hu, P. M. Petroff, and A. Imamoglu, Science **308**, 1158 (2005).
[11] W. C. Stumpf, M. Fujita, M. Yamaguchi, T. Asano, and S. Noda, Appl. Phys. Lett. **90**, 231101 (2007).
[12] J. Vučković, M. Lončar, H. Mabuchi, and A. Scherer, Phys. Rev. E **65**, 016608 (2001).
[13] I. P. Kaminow, T. Li, and A. Willner, *Optical Fiber Telecommunications V A: Components and Subsystems, B: Systems and Networks*, 5th ed. (Elsevier/Academic Press, New York, 2008).
[14] S.-H. Kim, S.-K. Kim, and Y.-H. Lee, Phys. Rev. B **73**, 235117 (2006).
[15] M. Larqué, T. Karle, I. Robert-Philip, and A. Beveratos, New J. Phys. **11**, 033022 (2009).
[16] E. Miyai, K. Sakai, T. Okano, W. Kunishi, D. Ohnishi, and S. Noda, Nature (London) **441**, 946 (2006).
[17] J.-H. Kang, M.-K. Seo, S.-K. Kim, S.-H. Kim, M.-K. Kim, H.-G. Park, Kim Ki-Soo, and Lee Yong-Hee, Opt. Express **17**, 6074 (2009).
[18] Nguyen-Vi-Quynh Tran, S. Combrié, and A. De Rossi, Phys. Rev. B **79**, 041101 (2009).
[19] C. Sauvan, G. Lecamp, P. Lalanne, and J. P. Hugonin, Opt. Express **13**, 245 (2005).
[20] P. Velha, E. Picard, T. Charvolin, E. Hadji, J.-C. Rodier, P. Lalanne, and D. Peyrade, Opt. Express **15**, 16090 (2007).
[21] A. Taflove and S. C. Hagness, *Computational Electrodynamics: The Finite-Difference Time-Domain Method*, 2nd ed. (Artech House, Boston, London, 2000).
[22] J.-P. Berenger, J. Comput. Phys. **114**, 185 (1994).
[23] A. Farjadpour, D. Roundy, A. Rodriguez, M. Ibanescu, P. Bermel, J. D. Joannopoulos, S. G. Johnson, and G. W. Burr, Opt. Lett. **31**, 2972 (2006).
[24] J. Vučkovič, M. Lončar, H. Mabuchi, and A. Scherer, IEEE J. Quantum Electron. **38**, 850 (2002).
[25] L. Stabellini, M. Carras, A. De Rossi, and G. Bellanca, IEEE J. Quantum Electron. **44**, 905 (2008).

[26] T. Yoshie, A. Scherer, J. Hendrickson, G. Khitrova, H. M. Gibbs, G. Rupper, C. Ell, O. B. Shchekin, and D. G. Deppe, Nature (London) **432**, 200 (2004).
[27] M. Notomi, A. Shinya, S. Mitsugi, G. Kira, E. Kuramochi, and T. Tanabe, Opt. Express **13**, 2678 (2005).
[28] Y. Akahane, M. Mochizuki, T. Asano, Y. Tanaka, and S. Noda, Appl. Phys. Lett. **82**, 1341 (2003).
[29] Z. Zhang and M. Qiu, Opt. Express **12**, 3988 (2004).
[30] G.-H. Kim, Y.-H. Lee, A. Shinya, and M. Notomi, Opt. Express **12**, 6624 (2004).